P9.7 DOPPLER LIDAR OBSERVATIONS OF INTERNAL GRAVITY WAVES, SHEAR INSTABILITY AND TURBULENCE DURING CASES-99

R.K. Newsom*, R.M. Banta[a], J. Otten[b], W.L. Eberhard[a], J.K. Lundquist[c]
*CIRA, Colorado State University, Fort Collins, CO
[a]NOAA/ETL, Boulder, CO
[b]Science and Technology Corporation, Hampden, VA
[c]University of Colorado, Boulder, CO

1. INTRODUCTION

Documentation of the evolution of internal gravity waves, Kelvin-Helmholtz shear instabilities and turbulence events in the stable nocturnal boundary layer (SBL) were principal scientific goals of the CASES-99 field observation program (Poulos et al. 2000). During its month-long deployment at the CASES-99 field site the NOAA/ETL High Resolution Doppler Lidar (HRDL) provided data on the structure and evolution of waves, shear instabilities and turbulence in the SBL. In this paper we examine two particular events in which wave-like structures were observed by the lidar. One-dimensional wavenumber spectra of the streamwise velocity component are computed as functions of height above ground, z. This provides information about the z dependence of the principle wavelengths and their amplitudes.

2. INSTRUMENTATION

HRDL is a coherent Doppler lidar that was specifically designed for atmospheric boundary layer research (Grund et al. 2000; Wulfmeyer et al. 2000). This instrument operates at a wavelength of $2\mu m$, a pulse repetition frequency of 200Hz, and a pulse length of 30m. HRDL measures range resolved profiles of aerosol backscatter intensity and Doppler or radial velocity. During the CASES-99 the maximum range of HRDL was typically between 2 to 3km.

3. OBSERVATIONS

During the CASES-99 field experiment HRDL recorded data on a total of 15 nights between October 4 and October 28, 1999. Currently, we have been able to identify three events in which highly coherent propagating

*Corresponding author address: Rob Newsom, NOAA/ETL/ET2, 325 Broadway, Boulder, CO 80303. Email: rnewsom@etl.noaa.gov.

waves were observed in the radial velocity field, unambiguously. For two of these events waves were observed in the shear zone between the surface and the low-level jet maximum. Both of these events were episodic and short-lived. For the third event, longer period oscillations were observed well above the low-level jet maximum (Worthington et al. 2000).

Although oscillations were commonly observed in the shear zone between the surface and the low-level jet, these oscillations usually did not exhibit a high degree of spatial or temporal coherence. Apparent wave-like structures that were observed during one scan would not maintain their continuity in subsequent scans.

In this paper we examine two specific events. Case 1 is an example of a highly coherent wave event, which was observed during the second intensive operation period. This event persisted for approximately 30 minutes. Case 2 is an example of a more common "wave event" in which very little correlation in the flow structure was observed from scan to scan. This activity persisted for several hours; however, for case 2 we analyze only a nine-minute subset. The times and dates of these two events are given in TABLE 1.

TABLE 1. CASES-99 cases

Case	Date (UTC)	Time (UTC)	
		Start	End
1	10/6/99	05:25:13	05:42:07
2	10/25/99	04:07:00	04:15:58

For both case 1 and case 2 the lidar performed shallow range-height-indicator (RHI) scans in the direction of the mean flow. An RHI scan is performed by scanning the laser beam in elevation while maintaining a fixed azimuth. For case 1 the lidar scanned between 0° to 10° in elevation at rate of $0.33^o s^{-1}$, resulting in a scan period of 1min. For case 2 the lidar scanned between 0° to 10° in elevation at rate of $0.8^o s^{-1}$, resulting in a scan

period of 30s. Radial velocity estimates were obtained by processing the raw heterodyne signals using 60m range gates and 50 pulse averages. As a result, the angular resolutions are 0.083^{o} and 0.2^{o} for cases 1 and 2, respectively.

4. ANAYLSIS

FIG. 1 shows a single RHI scan of the streamwise velocity component from case 1. This scan clearly shows relatively coherent oscillations in the flow between 40 m and 70 m above the surface. A low-level jet maximum of about 10ms^{-1} occurs at z≈120m.

The streamwise velocity field shown in FIG. 1 is obtained by dividing the radial velocity by the cosine of the elevation angle. This approximation to the streamwise velocity is valid as long as the elevation angle remains small and the streamwise component is much larger than the vertical component.

Velocities corresponding to low signal to noise ratios or hard target returns are edited out. The streamwise field is interpolated to a regular Cartesian grid using an exponential filter. The grid resolution is 40m in the horizontal direction and 5m in the vertical direction. The interpolating filter essentially removes energy in wavenumbers greater than 0.05m^{-1} in the horizontal direction and 0.4m^{-1} in the vertical direction. This is based on 50% of the filter's spectral maximum.

For each level one-dimensional spatial frequency spectra are computed from the space series formed by cross sections of constant z (see FIG. 1). The mean and any linear trend in the cross section is removed. A Hanning window is applied to further reduce spectral leakage effects. The resulting series is then zero padded up to the next highest power of two and Fourier transformed using an FFT algorithm. Spectral energy contained within frequency components below the minimum spatial frequency, as determined by the series length, is set equal to zero. The power spectra are then renormalized such that the total spectral energy equals the variance of the linearly detrended space series. These computations are repeated for each z level in a given scan.

There can be significant variation in the power spectra from scan to scan. In order to identify dominant spectral features the power spectra from all scans in the sequence are averaged. The resulting average spectra are then normalized by their maximum value and plotted in contour on a logarithmic scale.
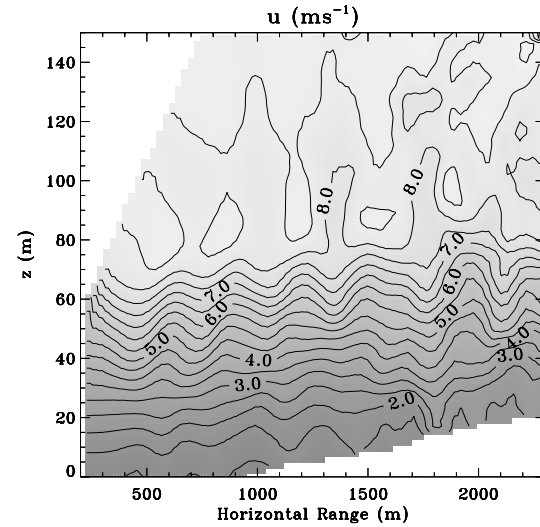

FIG. 1. A sample vertical cross-section of the streamwise velocity field for case 1.

4.1 *Case 1*

FIG. 2a shows the average power spectra for case 1. These spectra were obtained by averaging approximately 30 individual scans. A spectral maximum is indicated at a wavenumber of k≈0.017m^{-1}, corresponding to a wavelength of λ≈370m. This wave energy is highly concentrated between z≈55m and 70m. Between z≈70m and 85m the spectrum is characterized by a large negative gradient at k≈0.017m^{-1}. Above 85m we note the presence of a weak ridge in the spectrum which extends upwards toward the plot's upper boundary. This is consistent with the weak oscillations that were observed in this region.

FIG. 2b shows the mean and standard deviation of the streamwise velocity for case 1. The maximum standard deviation occurs at z≈60m, which corresponds to the location of the spectral peak. Above this point the standard deviation decreases quickly and then levels out where the low-level jet is strongest. The minimum standard deviation is achieved at the surface.

The mean streamwise velocity profile is characterized by an almost linear increase with height up to z≈80m. Above this level the profile remains relatively constant up to z≈140m.

The phase velocity was estimated to be between 5 to 7ms^{-1}. This is a qualitative estimate based on a visual inspection of successive scans.
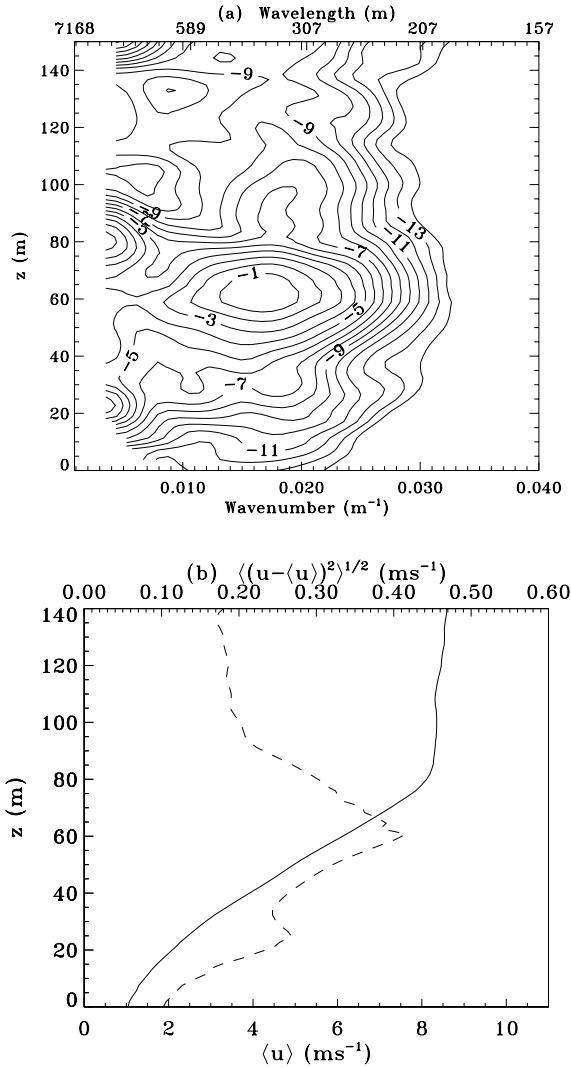

FIG. 2. (a) 1D power spectra as functions of z and wavenumber for case 1. (b) The mean streamwise velocity (solid line) and the standard deviation of the streamwise velocity (dashed line) for case 1.

4.2 Case 2

FIG. 3 shows a contour image of the streamwise velocity component for case 2. The flow is characterized by several large amplitude oscillations, which extend nearly throughout the depth of the shear layer. These oscillations weaken considerably above $z \approx 110$m. A low-level jet maximum of about 14ms^{-1} occurs at $z \approx 130$m.
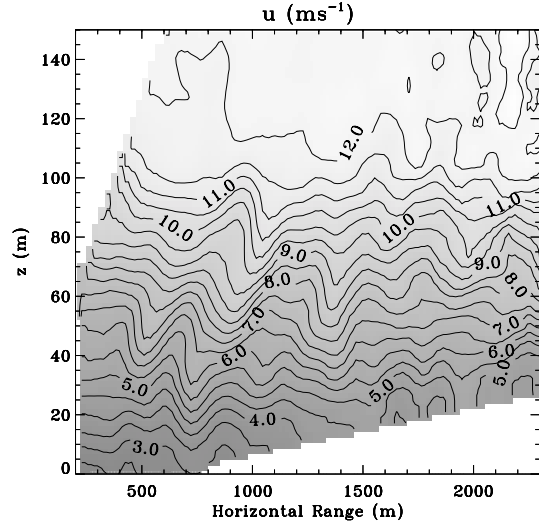

FIG. 3. A sample vertical cross-section of the streamwise velocity field for case 2.

As in case 1 power spectra as functions of wavenumber and z are averaged over approximately 30 RHI scans. From FIG 4a we see a slight indication of a spectral maximum at $z \approx 70$m and a wavenumber of $k \approx 0.013$m^{-1}, corresponding to a wavelength of $\lambda \approx 480$ m. The wave energy near this maximum is not as concentrated in the vertical direction as it was in case 1. There is a very steep negative gradient in the spectrum between $z \approx 90$ and 110m. In this region the energy drops by roughly 8 dB at $\lambda \approx 480$ m. above 110 m the spectrum is relatively flat.

The mean streamwise velocity and its standard deviation (FIG. 4b) appear qualitatively similar to case 1 (FIG. 2b). As in case 1 the maximum in the standard deviation profile coincides with the spectral peak. However, for case 2 the standard deviation profile achieves its minimum value above the shear zone (for $z > 110$m).

It was difficult to obtain a reliable estimate of the phase velocity of the oscillations in case 2. Despite a relatively fast scan period of 30s little correlation was observed from scan to scan.

Shortly after recording the sequence of RHI scans for case 2 the lidar performed a series of low elevation angle sector scans into the general wind direction. One sample scan from this sequence is shown in FIG. 5. Rather than a classic two-dimensional wave pattern, this scan shows a slight tendency of the velocity structures to be elongated in the direction of the mean flow.
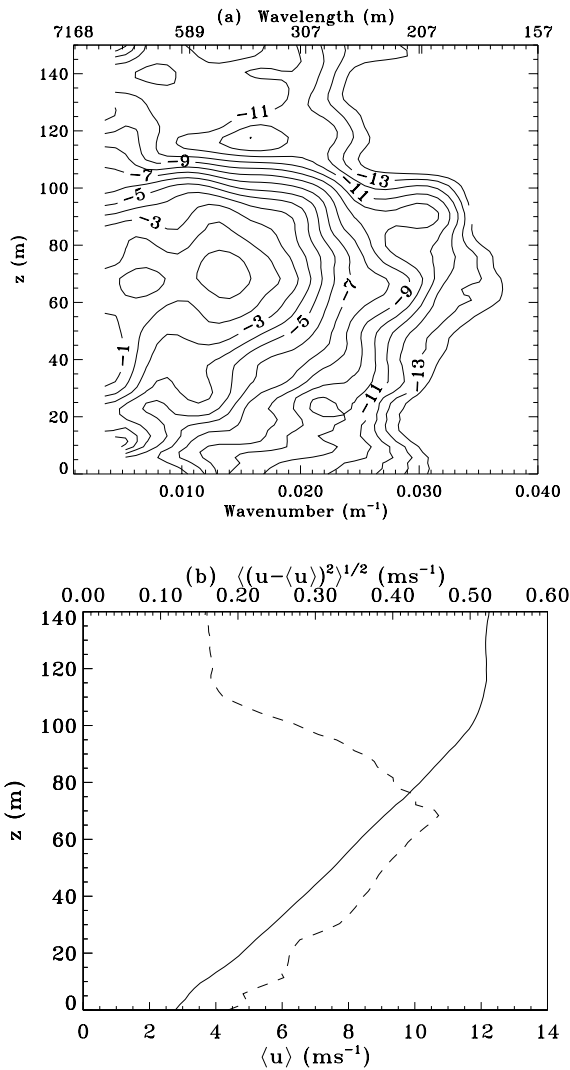
FIG. 4. (a) 1D power spectra as a function of z and wavenumber for case 2. (b) The mean streamwise velocity (solid line) and the standard deviation of the streamwise velocity (dashed line) for case 2.

5. SUMMARY

We have examined the structure of spatial frequency spectra of streamwise velocity fluctuations under stable nocturnal conditions. Two somewhat similar cases were considered. In both cases a low-level jet was present with maximum wind speeds situated between 110 to 140 m above the surface. In case 1 the oscillations in the streamwise field were highly coherent and confined to a relatively thin layer. In case 2 the fluctuations were less coherent and extended nearly throughout the depth of the shear layer. In both cases spectral energy achieves a maximum well below the "nose" of the jet and then decreases dramatically above this point. However, for case 2 the spectral maximum was not as well defined as in case 1.

The analysis presented here is an initial step to a more comprehensive study. Further analysis will incorporate information from other sensors.
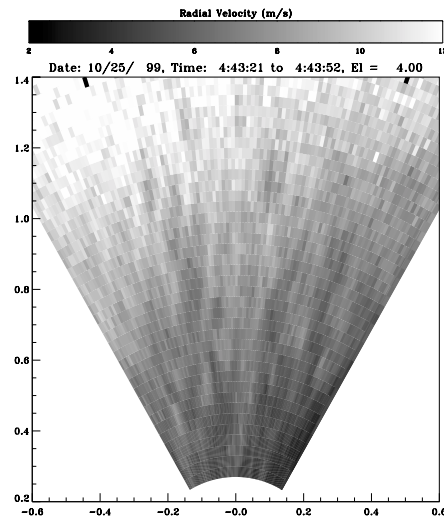

FIG. 5. A sample horizontal cross-section of the radial velocity field recorded at approximately 04:43:40 on 10/25/99 (UTC). The horizontal (east-west) and vertical (north-south) axes are given in kilometers from the lidar.

REFERENCES

Grund C. J., R. M. Banta, J. L. George, J. N. Howell, M. J. Post, R. A. Richter, and A. M. Weickmann, 2000: High-resolution Doppler lidar for boundary layer and cloud research. *J. Atmos. Oceanic Technol.*, accepted for publication.

Poulos G. S., D. C. Fritts, W. Blumen, W. D. Bach, 2000: CASES-99 field experiment: an overview. *14th Symposium on Boundary Layers and Turbulence,* Aspen, CO.

Worthington R. M., R. M. Banta, R. K. Newsom, J. K. Lundquist, M. L. Jensen, A. Muschinski, R. G. Frehlich, B. B. Balsley, 2000: Combined lidar and in-situ measurements of waves in the stable night-time boundary layer above Kansas. *14th Symposium on Boundary Layers and Turbulence,* Aspen, CO.

Wulfmeyer, V., M. Randall, W. A. Brewer, R. M. Hardesty, 2000: 2-μm Doppler lidar transmitter with high frequency stability and low chirp. *Opt. Lett.*, accepted for publication.